Pergamon

PII: S0003-4878(99)00091-5

Ann. occup. Hyg., Vol. 44, No. 3, pp. 191–202, 2000

Printed in Great Britain.
0003–4878/00/$20.00

On the Use of Computational Fluid Dynamics in the Prediction and Control of Exposure to Airborne Contaminants—an Illustration Using Spray Painting

MICHAEL R. FLYNN†* and ERIC D. SILLS‡

†*Department of Environmental Sciences and Engineering, University of North Carolina, Chapel Hill, NC* 27599-7400, *USA*; ‡*North Carolina Supercomputing Center, PO Box* 12889, *RTP, NC* 27709-2889, *USA*

Computational fluid dynamics (CFD) is employed to simulate breathing-zone concentration for a simple representation of spray painting a flat plate in a cross-flow ventilated booth. The results demonstrate the capability of CFD to track correctly changes in breathing-zone concentration associated with work practices shown previously to be significant in determining exposure. Empirical data, and models verified through field studies, are used to examine the predictive capability of these simulations and to identify important issues in the conduct of such comparisons. A commercially available CFD package is used to solve a three-dimensional turbulent flow problem for the velocity field, and to subsequently generate particle trajectories for polydisperse aerosols. An in-house algorithm is developed to convert the trajectory data to breathing-zone concentrations, transfer efficiencies and aerosol size distributions. The mesh size, time step, duration of the simulation, and number of particles per size interval are all important variables in achieving convergent results.

Keywords: computational fluid dynamics; spray painting; ventilation; exposure modelling

NOMENCLATURE

C	total mass concentration in the breathing zone
U	average air velocity in the cross-flow spray booth
H and D	height and breadth of the worker
m_o	over-spray generation rate
F_g	momentum flux of air from the gun
F_m	momentum flux of air through the projected area of the mannequin
Θ	angle of orientation
$\mathbf{u}$	air velocity vector
$\mathbf{v}$	particle velocity vector
Re_p	particle Reynolds number
C_D	particle drag coefficient
μ_t	eddy viscosity
k	turbulence kinetic energy
ε	dissipation due to turbulence
Φ	viscous dissipation function
τ	particle relaxation time
μ	coefficient of laminar viscosity for air
α_0	diffusivity of air in air
ρ	density

Received 11 February 1999; in final form 6 August 1999.
*Author to whom correspondence should be addressed. Tel.: +1-919-966-3473; Fax: +1-919-966-7911; E-mail: mike_flynn@unc.edu

INTRODUCTION

Numerical simulation plays an important role in the analysis of many complex real-world problems, (for example, weather forecasting), and in the design of modern conveniences (cars and airplanes). The use of such simulations by occupational hygienists to optimise contaminant control decisions is the focus of this paper. Although numerical simulations of local exhaust and dilution ventilation problems have been underway for years (Heinsohn *et al.*, 1982; Nielsen *et al.*, 1978), there are many unanswered questions about how to use this technology effectively; and few, field-based examinations of such simulations (Heinonen *et al.*, 1996; Andersson and Alenius, 1997).

Computational fluid dynamics (CFD) is a scientific discipline devoted to the study of numerical (approximate) solutions for the equations governing fluid motion. Over the past decade enormous progress has been made in this field, and a wide variety of methods exist to simulate a host of problems. The foundations of CFD are the first principles of mass, momentum, and energy conservation.

To conduct a numerical simulation using CFD a simplified abstraction of reality must be created that is compatible with the computer program. This conceptual model is the first in a series of approximations that are invoked. If the conceptual model is not a sufficient representation of reality with regard to the desired outcome, then no matter how accurate the simulation, the results will be of limited value. Conversely, a good conceptual model will be inadequate, if there is insufficient numerical resolution. A balance between these two components is essential to achieve meaningful results given finite resources.

Contaminant control interventions are implemented to reduce exposure, that is, the time weighted average breathing-zone concentration. To be a useful analytical tool, CFD simulations must, at a minimum, track changes in breathing-zone concentration as they occur in reality. Although accurate quantitative predictions of exposure are desirable, a correct rank ordering is a useful beginning, particularly for discriminating between alternative control interventions (Kulmala *et al.*, 1996). This work examines the ability of CFD to track exposure differences that result from spray painting a flat plate in a cross-draft booth as a function of a specific work practice, that is, the orientation of spraying with respect to booth air flow. This effect has been identified in both laboratory and field studies (Carlton and Flynn, 1997a; Heitbrink *et al.*, 1995) as a significant determinant of exposure.

The numerical simulations presented here are preliminary in nature and do not represent a definitive CFD analysis of the problem. They are intended to support a basic conceptual approach and to identify significant issues for further study. Issues related to the accuracy, use, validation and feasibility of such simulations are discussed. The simulations were conducted using the FIDAP® finite element computer package (FIDAP, 1995). The computer-predicted ranking of breathing-zone concentrations correctly tracked those measured in a wind tunnel facility.

BACKGROUND

A recent study (Flynn *et al.*, 1999) presented a conceptual model of exposure for compressed air spray painting applications. It emphasised the dependence of exposure on the over-spray generation rate of aerosol, and the air velocity field transporting it to the breathing zone. The model is based on dimensional analysis and empirical data gathered in scale model wind tunnel studies. Field studies confirmed its applicability and provided an estimate of the uncertainty in using such an approach for real-world prediction (Carlton and Flynn, 1997b). The model, as summarised in Eq. (1), predicts a dimensionless breathing-zone concentration as a function of an air momentum flux ratio and worker orientation.

$$\frac{CHUD}{m_o} = f\left(\frac{F_g}{F_m}; \Theta\right) \tag{1}$$

where C is the total mass concentration in the breathing zone, U is the average air velocity in the cross-flow spray booth, H and D are the height and breadth of the worker, m_o is the over-spray generation rate, F_g and F_m are the momentum flux of air from the gun, and through the projected area of the mannequin, respectively. Θ is the angle of orientation (see Fig. 1), and

$$\frac{F_g}{F_m} = \frac{K}{HDU^2} \tag{2}$$

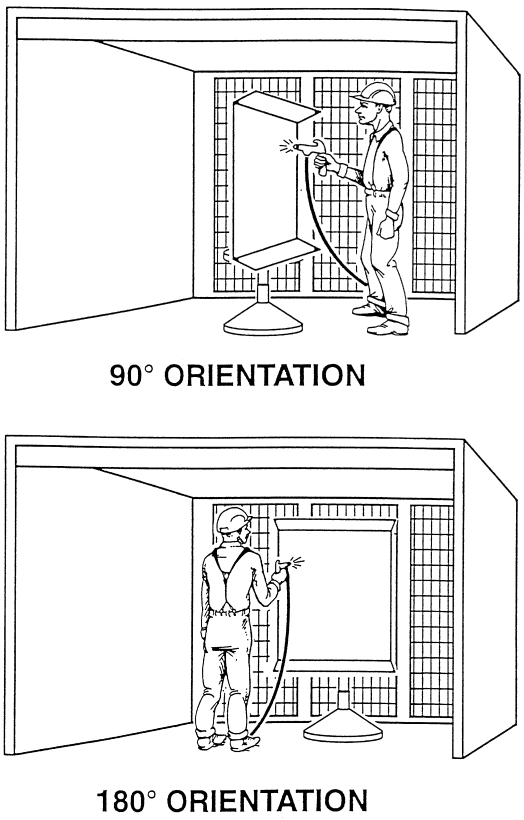

Fig. 1. The reality simulated: spray painting a flat plate in a ventilated booth.

where

$$K = \frac{\rho_n A_n V_n^2 + (p_n - p_{atm})A_n}{\rho_{atm}} + \frac{\rho_f A_f V_f^2 + (p_f - p_{atm})A_f}{\rho_{atm}} \quad (3)$$

K is the kinematic momentum flux of air from the spray gun, p is pressure, V is the air velocity, A is the exit area, and the n and f subscripts distinguish between the nozzle atomisation air flow and nozzle fan air flow (used to shape the spray pattern), respectively. The inclusion of the pressure difference terms in Eq. (3) reflects the contribution to momentum when air velocities are sonic, mass flow is choked, and nozzle/fan exit pressure is greater than atmospheric. For the $\frac{1}{4}$ J nozzle investigated here there is no fan air, hence the second term on the right hand-side is 0.

Equation (1) indicates that a dimensionless breathing-zone concentration is a function of a dimensionless momentum flux ratio, and the orientation of the worker and spray gun within the cross-flow booth. It does not specify the form of the function, which was deduced from experimental wind-tunnel data (Flynn *et al.*, 1999) as:

$$\log_{10}\left(\frac{CHUD}{m_o}\right) = \alpha + \Delta\left(\frac{F_g}{F_m}\right)^{\gamma} \quad (4)$$

where α, Δ, and γ are constants dependent on geometry and orientation.

The wind-tunnel experiments were conducted using a 1.04-m tall store mannequin, 0.2 m wide at the chest, using a $\frac{1}{4}$ J Spray Systems nozzle to spray corn oil at a flat plate 0.66 m wide by 1.02 m tall. The spray nozzle was 0.2 m from the plate and was operated at gauge air pressures of 138–345 kPa (20–50 psig), corresponding to air mass flow rates of 0.00106–0.002 kg s^{-1}. Corn oil was sprayed in lieu of paint to give air-to-liquid mass flow ratios of 0.7–1.3. Wind tunnel air speeds varied from 0.381 to 1.016 m s^{-1} and spraying was conducted in the two different orientations shown in Fig. 1. For this specific geometry, the constants were determined and the exposure model specified as:

$$\log_{10}\left(\frac{CHUD}{m_o}\right)_{90} = -0.796 - 5.37\left(\frac{F_g}{F_m}\right)^{-1.58} \quad (5)$$

$$\log_{10}\left(\frac{CHUD}{m_o}\right)_{180} = -2.3 + 0.8\left(\frac{F_g}{F_m}\right)^{-1} \quad (6)$$

The utility of CFD as a tool in optimising control interventions requires, at a minimum, the correct ranking of exposures for the alternative scenarios. If the ratio of exposures is also simulated correctly, valuable additional information is obtained. The most rigorous verification of a CFD prediction is actually matching the measured value, within the uncertainties of both the measurement and the simulation. The empirical model outlined above suggests that once the over-spray generation rate (m_0) is known, the geometry, orientation, and momentum flux ratio determine the transport, and hence the dimensionless breathing-zone concentration, $CHUD/m_o$. The determination of the over-spray generation rate, requires calculation of the transfer efficiency, that is, the fraction of mass that deposits on the plate. This is an impaction problem (Flynn *et al.*, 1999; Kwok 1991) once the air flow field and particle size distribution are specified.

The dependent variables of interest are: (1) the breathing-zone concentration, (2) the aerosol size distribution, and (3) the transfer efficiency of the spraying process. Two specific experiments reported in Carlton and Flynn (1997a) were selected for numerical simulation using the FIDAP finite element program. These experiments were identical, except for the orientation, and employed the $\frac{1}{4}$ J nozzle operating at a gauge air pressure of 345 kPa (50 psig), a wind tunnel air speed of 0.478 m s^{-1}, and a liquid mass flow of 0.00283 kg s^{-1}.

NUMERICAL METHODS

The purpose of this study is threefold. (1) First is to solve the three-dimensional, incompressible, steady-state, turbulent flow problem for the air velocity field. A passive tracer species is also included to track the jet-air. (2) Once the velocity field is specified, aerosol particles are introduced at the centre of the jet face and tracked through the flow field. The aerosol sizes input to the code are determined from an empirical equation specific to the nozzle used here (Kim and Marshall, 1971). (3) Finally, the particle trajectories generated in this fashion are converted into transfer efficiency predictions, breathing-zone mass concentrations and size distributions for comparison to the empirical data. The first two steps are accomplished using the FIDAP (v8.0) finite element program. Step three is accomplished through the development of an in-house algorithm to post-process the trajectory output.

Part of any numerical simulation is selecting the physical geometry to approximate the reality. Here a circular cylinder of height H and diameter D is used to represent the mannequin (worker). A square orifice on the surface of the cylinder of side length, s, is used to represent the spray nozzle as a jet of air. The face of this nozzle is at a distance, Z_p, from the plate. A comparison of experimental and computational length, velocity, and mass flow scales is given in Table 1.

In reality the $\frac{1}{4}$ J nozzle has an area for air flow of 0.0225 cm^2 and the air velocity at the exit is

Table 1. Experimental and numerical parameters

	Experimental values	Simulations
D (m)	0.2	0.203
H (m)	1.04	1.016
s (m)	0.0015	0.0254
Z_p (m)	0.203	0.254
L_t length of tunnel (m)	2.44	6.07
W_t width of tunnel (m)	1.52	1.524
H_t height of tunnel (m)	1.52	1.524
H_p plate (m)	1.02	1.016
W_p plate (m)	0.66	0.66
U_j jet velocity (m s^{-1})	sonic	35.56
U tunnel velocity (m s^{-1})	0.478	0.254
m_a jet mass flow (kg s^{-1})	0.002	0.023
m_t tunnel (kg s^{-1})	1.33	0.59
m_L (kg s^{-1})	0.00285	N/A
F_g/F_m	18.2	18

sonic. This leads to computational difficulties since mesh requirements become prohibitive at such disparate length scales; and compressible flow exists over a small region in front of the nozzle with incompressible flow over the vast majority of the domain. Empirical work (Flynn *et al.*, 1999) using an HVLP spray gun (a much larger nozzle exit area and subsonic discharge velocities) suggests that the momentum flux ratio should be predictive of the dimensionless concentration if the length scales are close. This work relies on an incompressible flow calculation using a larger orifice, but equivalent momentum–flux ratio, to approximate a compressible-flow, high-pressure spraying operation with a much smaller orifice.

Air flow field

The equations governing the air flow are the steady-state, incompressible, turbulent, Navier Stokes equations with the standard two-equation k–e model to calculate the turbulent viscosity. A species transport equation, Eq. (9), is also included to calculate the concentration field for a passive tracer. These equations, in vector form, are:

$$\nabla \cdot \mathbf{u} = 0 \tag{7}$$

$$\mathbf{u} \cdot \nabla \mathbf{u} = \nabla \cdot \left[\frac{\mu + \mu_t}{\rho} (\nabla \mathbf{u} + \nabla \mathbf{u}^T) \right] - \frac{1}{\rho} \nabla p \tag{8}$$

$$\mathbf{u} \cdot \nabla C = \nabla \cdot [\alpha \nabla C] \tag{9}$$

$$\rho(\mathbf{u} \cdot \nabla k) = \nabla \cdot \left(\mu + \frac{\mu_t}{\sigma_k} \nabla k \right) + \mu_t \Phi - \rho \varepsilon \tag{10}$$

$$\rho(\mathbf{u} \cdot \nabla \varepsilon) = \nabla \cdot \left(\mu + \frac{\mu_t}{\sigma_\varepsilon} \nabla \varepsilon \right) + c_1 \frac{\epsilon}{k} \mu_t \Phi - c_2 \rho \frac{\varepsilon^2}{k} \tag{11}$$

where

$$\mu_t = \rho c_\mu \frac{k^2}{\varepsilon} \tag{12}$$

$$\alpha = \alpha_0 + \frac{\mu_t}{\rho S_t} \tag{13}$$

The constants are: $c_\mu = 0.09$; $\sigma_k = 1.00$; $\sigma_\varepsilon = 1.30$; $c_1 = 1.44$; $c_2 = 1.92$; $S_t = 0.9$ and for air $\alpha_0 = 0.0000194$.

These equations, along with the boundary conditions specified in Table 2, are solved with FIDAP using the segregated approach with pressure projection. Streamline upwinding is employed together with the cell Reynolds/Peclet number relaxation scheme. The nominal criterion for terminating the non-linear iteration loop is convergence of the L2 relative error norm to below 0.001 for all variables simultaneously. This level was achieved on all 90° simulations, however, the two finest meshes in the

Table 2. Nominal boundary conditions for Eqs (7)–(11)

	Tangential velocity (m s^{-1})	Normal velocity (m s^{-1})	Stress	Turbulence kinetic energy (m s^{-1})^2	Turbulence dissipation (m^2)/(s^3)$^{-1}$	Species concentration mole fraction
Inlet	0	0.254	–	0.01551	0.01431	0
Outlet	–	–	0	Dn = 0[a]	Dn = 0	Dn = 0
Jet face	0	35.56	–	64.5	20 400	1.0
Solid surfaces	0	0	0	0	0	0

[a]Dn = 0 indicates the normal derivative of the quantity is 0.

Table 3. Input particle size distribution

Size range (μm)	Midpoint (μm) input size to FIDAP	Mass fraction in interval
0–5	2.5	0.0274
5–10	7.5	0.0314
10–15	12.5	0.0356
15–20	17.5	0.0399
20–25	22.5	0.0440
25–30	27.5	0.0478
30–35	32.5	0.0512
35–40	37.5	0.0538
40–45	42.5	0.0556
45–50	47.5	0.0563
50–55	52.5	0.0560
55–60	57.5	0.0546
60–65	62.5	0.0522
65–70	67.5	0.0491
70–75	72.5	0.0454
75–80	77.5	0.0414
80–85	82.5	0.0371

180° case did not quite achieve this level. The two simulations, A and B were identical except for orientation (A = 90°, B = 180°).

Aerosol trajectories

The aerosol particles are tracked according to a generalised drag equation:

$$\frac{d\mathbf{v}}{dt} = \frac{\mathbf{u} - \mathbf{v}}{\tau} + \frac{\rho_p - \rho_a}{\rho_p}\mathbf{g} \tag{14}$$

where:

$$\tau = \frac{4\rho_p D_p^2}{3\mu C_D Re_p} \tag{15}$$

and

$$C_D = \frac{24}{Re_p}(1 + 0.15Re_p^{0.687}) \tag{16}$$

The particles are introduced into the flow field at the centre of the jet face, moving at the air velocity of the jet. The key parameters governing the numerical solution are: the size of the time step (Δt), the total time the particles are tracked (T), the input size distribution (Ψ), and the number of particles input in each size interval (N_i).

The input particle size distribution is calculated according to the empirical equations of Kim and Marshall (1971) who specifically examined the $\frac{1}{4}$ J nozzle. A discrete representation of the size distribution was constructed based on 5-μm intervals and the midpoint was used as input to the FIDAP code. The mass fractions associated with each size interval are also calculated, as they are important in determining transfer efficiency and exposure. Table 3 presents the discrete representation of the particle size distribution for the experimental conditions described above. The upper size of approximately 85 μm was selected since it was observed during the simulations that all particles greater than this size impacted on the plate and did not contribute to exposure. All of the mass over 85 μm is assumed to impact on the plate and is included in the simulated prediction of transfer efficiency.

Equation (14) is integrated with an implicit option available in FIDAP. At each time step a turbulent displacement of the particle is included based on the calculated turbulence parameters via a random number subroutine. This means that for repeated numerical simulations of exactly the same problem, different trajectories will result, that is, there is a statistical distribution of solutions. The FIDAP program allows an output file to be created, containing the endpoints of each increment of each particle trajectory, along with the value of the time step. This information was used to calculate transfer efficiency, breathing-zone concentration, and particle size distributions, as described below.

Table 4. Mesh refinement study

Total nodes in mesh	Mean tracer concentration in B.Z. 27 points (ppm)		L2 norms	
	90°	180°	90°	180°
46 000	100 000	156.0		
80 000	34 000	1.0	1.51	151.2
170 000	50 000	1.0	0.43	0.57

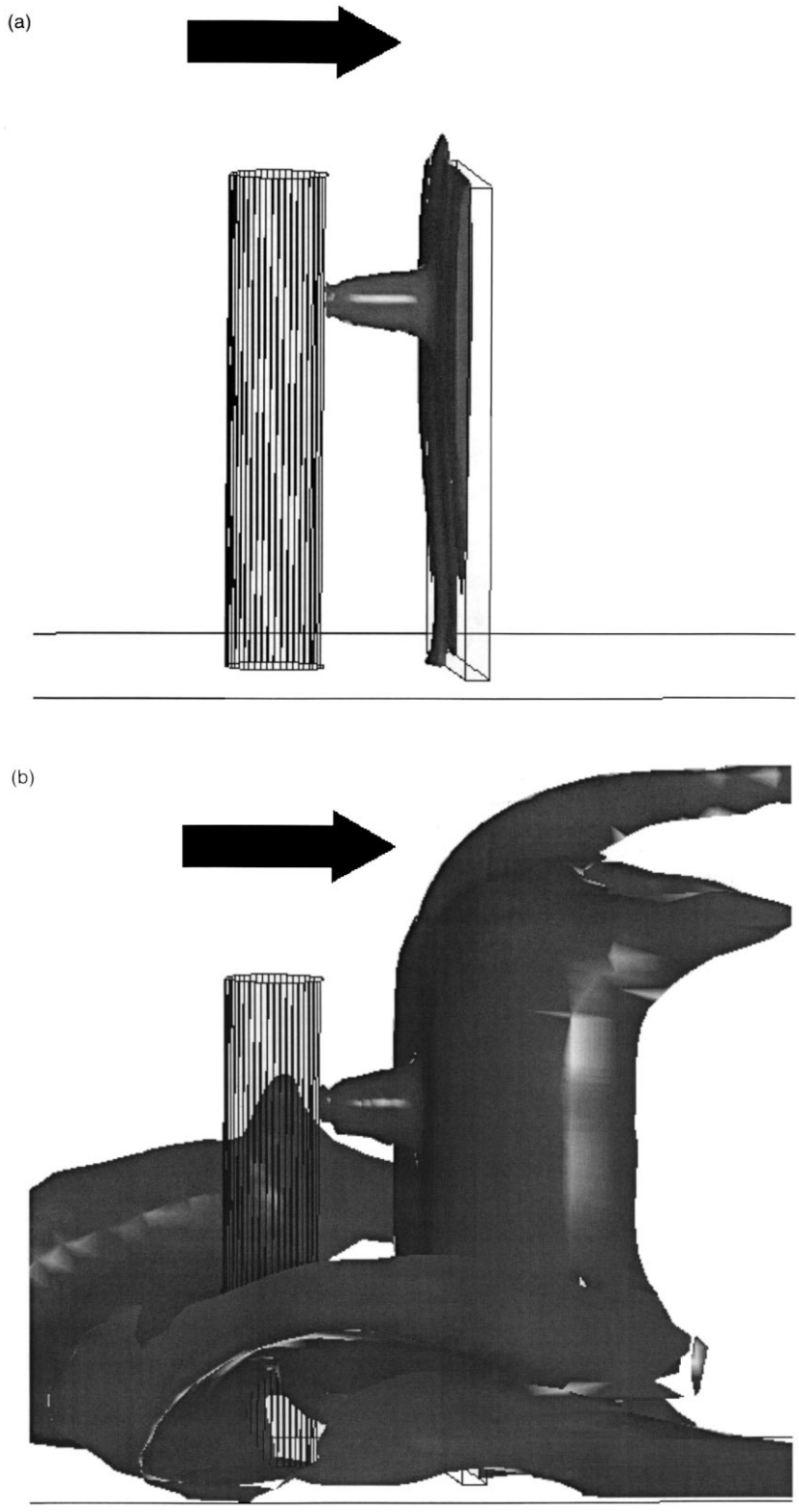

Fig. 2. Iso-concentration surfaces for the 180° simulation: (a) 0.125 and (b) 0.05—side views.

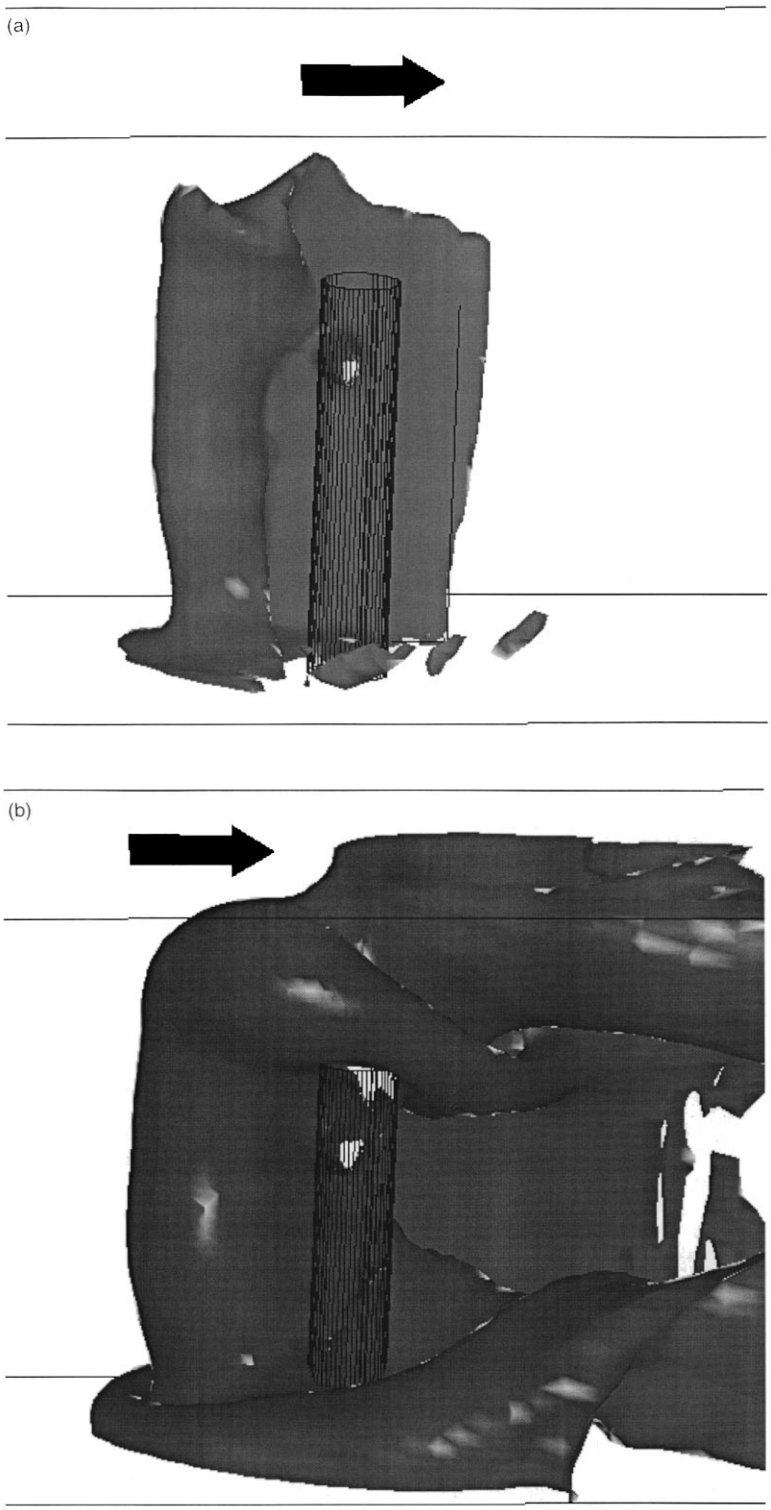

Fig. 3. Iso-concentration surfaces for the 90° simulation: (a) 0.125 and (b) 0.05—side views; (c) 0.125 and (d) 0.05—top-down views.

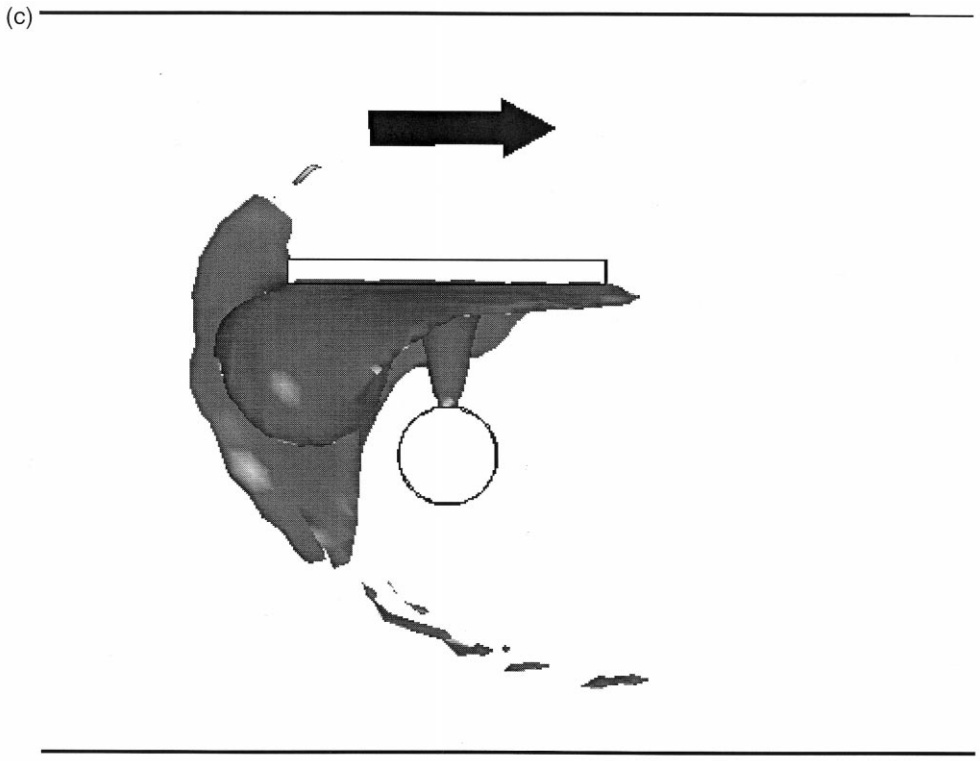

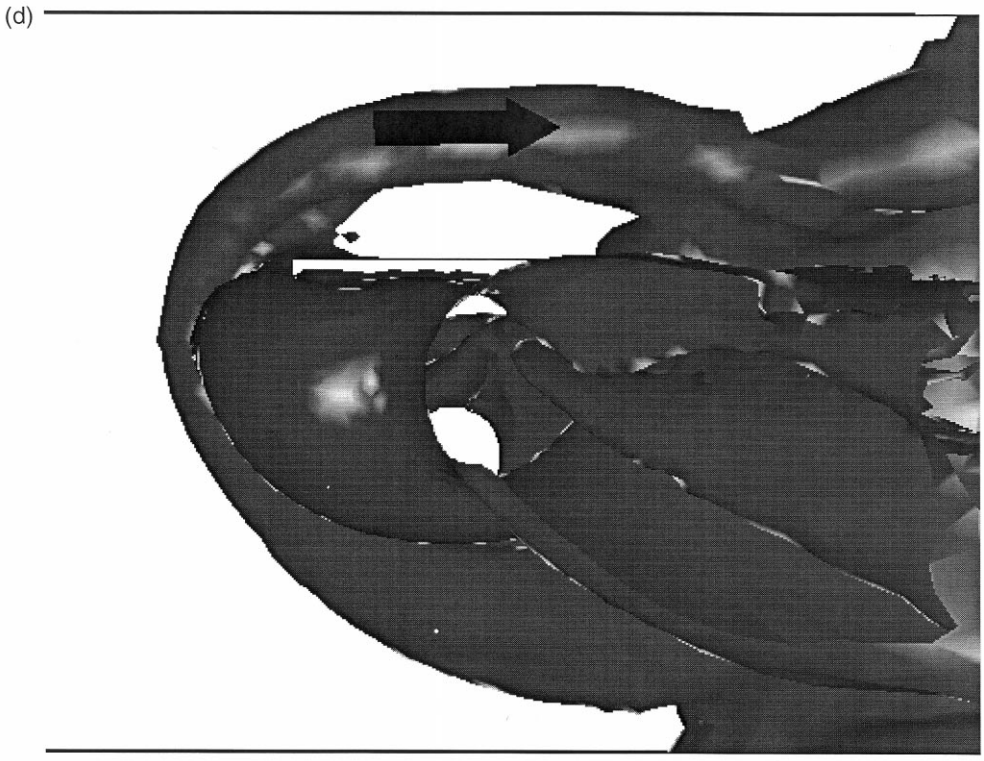

Fig. 3 (*continued*)

Transfer efficiency and concentration

The formula for the calculation of mass concentration in the breathing zone, based on particle trajectories determined from the computed velocity field, is given by Heinsohn (1991) as:

$$C = \sum_{i=1}^{N} \frac{m_i t_i}{V_{bz}} \tag{17}$$

where, m_i is the mass flow rate associated with the ith trajectory, V_{bz} is the breathing-zone volume, t_i is the residence time for the ith trajectory in V_{bz}, and N is the total number of trajectories. A FORTRAN code was written to generate a spherical breathing zone and calculate concentrations for each particle size selected. The volume of this numerical breathing zone, scaled to represent approximately one inhalation volume, is 0.000905 m^3 and is positioned to coincide with the location of the filter used in the experiment. The algorithm identifies the proportion of each trajectory increment that lies within the numerical breathing zone and sums the time spent within this zone based on linear interpolation. This provides the information for exposure and size distribution calculations.

Transfer efficiency is defined here as the fraction of mass sprayed that deposits on the object. Thus, transfer efficiency for a given size particle is obtained as the ratio of particles impacting on the object to the total number used for that size. Overspray generation rates by size interval are obtained by multiplying this transfer efficiency by the liquid mass flow rate and the mass fraction associated with the given size range. An additional part of the in-house post-processing code determines the number of aerosol particles impacting on the object.

RESULTS

Air velocity field and passive tracer

Part of any numerical simulation involves examining the truncation error that results from approximating the solution to a continuous problem on a finite mesh. This is done by refining the mesh, that is, increasing the number of nodes, until two successive meshes result in negligible differences in the dependent variables of interest. To examine this error we employed three different mesh densities for each of the two situations examined. A vector of tracer concentration consisting of 27 points, selected in the breathing zone, was taken as the solution variable to examine under mesh refinement. The L2 relative error norm of these 27 point concentrations as well as their average value are reported in Table 4 as a function of the number of nodes for each mesh. As the data indicate, the 180° case achieves a mesh independent value of 0.000001 whereas the 90° case shows oscillating convergence with a final value of 0.05 and some uncertainty. In each case significant reduction in the L2 norms indicates convergent behaviour.

Figure 2(a, b) presents the passive tracer iso-concentration surfaces of 0.125 and 0.05 (mole fractions), respectively, for the 180° position. Figure 3(a, b) shows the corresponding contours in the 90° position. Figure 3(c, d) shows an additional top-down view of the 0.125 and 0.05 contours shown in Fig. 3(a, b). The arrow indicates the direction of the booth air flow. The passive tracer is actually jet air and the concentrations represent the dilution of the jet that occurs as it is transported to the breathing zone. These visualisations clearly indicate the enhanced transport of the jet-air into the breathing zone in the 90° orientation relative to the 180° case. The CFD predictions of tracer breathing-zone concentration are presented in Table 5. The ranking of exposure based on the tracer results is correct, that is, A > B. In the 90° orientation (simulation A) the predicted breathing zone concentration of tracer is 0.05, while for the corresponding 180° simulation (B) a value of 0.000001 was obtained.

These tracer concentrations can be used to estimate dimensionless aerosol concentration if one assumes that the particles are transported similarly to the jet air. In this case it can be shown that

$$\frac{CHUD}{m_o} = \frac{C_t HUD}{Q_j} \tag{18}$$

where C_t is the tracer concentration and Q_j is the jet air flow. If this approach is employed, the calculated values for the dimensionless aerosol concen-

Table 5. Summary of simulated and empirical results

	Simulation results		Empirical results	
	A (90°)	B (180°)	A (90°)	B (180°)
Transfer efficiency	0.77	0.78	0.94	0.94
Overspray m_o (g s^{-1})	0.65	0.62	0.17	0.17
$CHUD/m_o$ (trajectories)	1.08	0	0.14	0.0055
$CHUD/m_o = C_t HUD/Q_j$	0.2	4 E-06	0.14	0.0055
MMD (μm)	22.9	N/A	25.6	15.0
GSD	1.9	N/A	1.6	1.4
Tracer concentration (mole fraction)	0.05	1 E-06	N/A	N/A

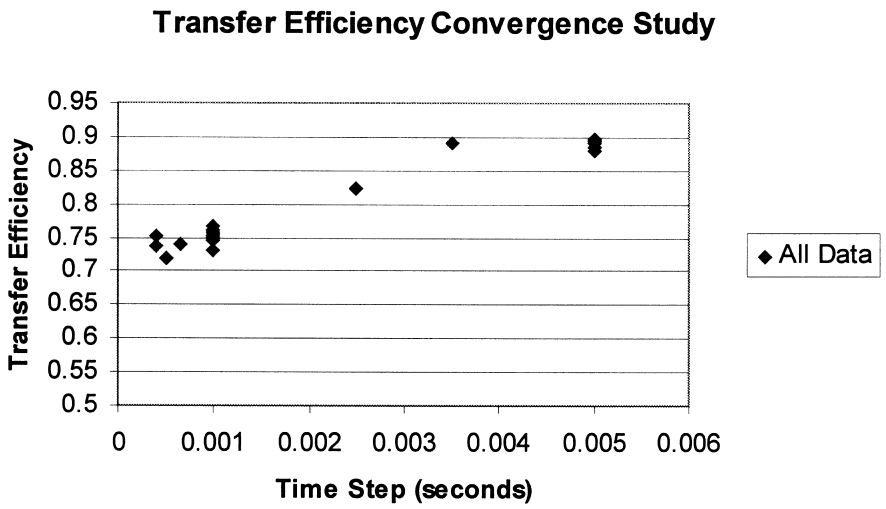

Fig. 4. Convergence results for transfer efficiency.

tration are 0.2 and 0.000004 for the 90° and 180° orientations, respectively. It is anticipated that this approach may provide reasonable estimates for very small particles, and progressively worse estimates for larger particles.

Transfer efficiency

The time step is the most critical variable governing transfer efficiency. Figure 4 presents a plot of predicted transfer efficiency as a function of time step. The figure contains data for both orientations, as there was little difference between the two positions. As the time step is reduced (by more than a factor of 10) the trajectory accuracy improves, and transfer efficiency converges to a value of approximately 0.75. The actual values obtained for transfer efficiency were 0.772 in the 90° case and 0.778 in the 180° position. Since computational resources increase dramatically with smaller time steps it was judged that a value of 0.001 s would be adequate for subsequent aerosol exposure simulations. This value for the time step is about 0.1 of the time scale based on the jet face velocity and the distance from the jet to the plate. The experimental values for transfer efficiency were 0.94 in each orientation.

Aerosol concentration and size distributions

Due to the turbulent nature of the flow, there is a distribution of solutions for any given input. In addition, the lower the concentration—the greater the number of trajectories needed, since the probability

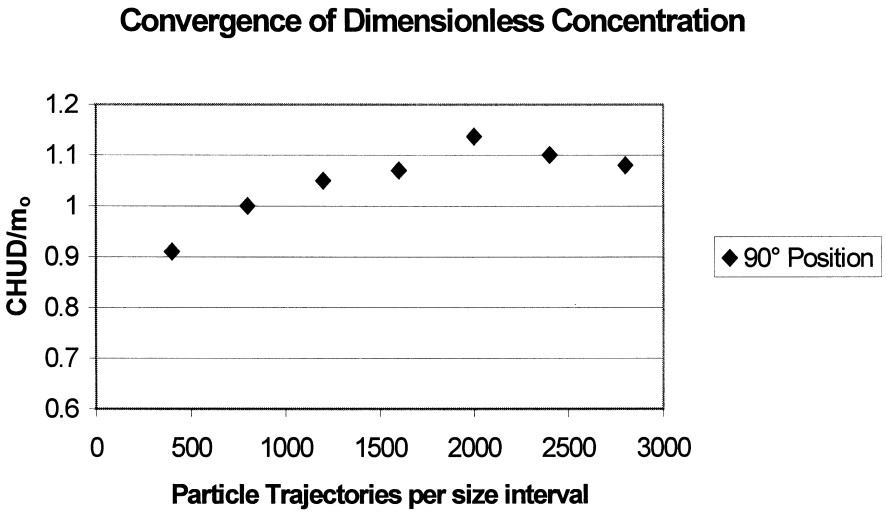

Fig. 5. Convergence results for dimensionless concentration.

of a trajectory intersecting the breathing zone decreases as concentration drops. Figure 5 presents the results of the convergence study for simulation A. The figure plots the dimensionless breathing zone concentration as a function of the total number of trajectories per size interval used in the simulation. The results suggest that for the 90° case the predicted dimensionless concentration is about 1.08. The comparable 180° simulation produced a result of 0, since no particles of any size were found in the breathing zone. The corresponding measured values of dimensionless concentration were 0.14 and 0.0055, respectively.

Convergent transfer efficiency was the governing criterion for selecting the time step. However, the duration of the simulation (T) is an important variable for concentration convergence. A period of 30 s, approximately three wind-tunnel volume air-changes, was found to be adequate. Approximately 90–95% of the particles used in the simulation had exited the domain of interest, and little difference was observed when a converged 40-s simulation was compared to a converged 30-s value. The duration of the simulation divided by the time step and multiplied by the number of trajectories used dictates the total memory needed by FIDAP to perform the trajectory calculations, which was half a gigabyte of RAM in the high-end simulations performed here.

A breathing-zone size distribution was constructed for the 90° case. The mass median diameter (MMD) was 23 μm and the GSD was 1.8. A summary of all the results is presented in Table 5. Experimental values are compared with simulation values for breathing-zone concentration, transfer efficiency, MMD, GSD, and dimensionless breathing-zone concentration.

In summary, the numerical simulations correctly identify the orientation effect observed in the experiment, higher exposure in the 90° case; however, the magnitude of the effect is overestimated using either the tracer gas concentration ratio or the aerosol concentration ratio. The predicted transfer efficiency of 0.77 is about 82% of the measured value of 0.94; however, this results in an overestimate for the mass generation rate by a factor of about four; that is, the computer simulation predicts almost four times the mass generation rate observed in the experiment. The mass median diameter observed experimentally in the 90° orientation was in reasonable agreement with the numerical simulation.

DISCUSSION

The CFD simulations presented here are approximate solutions to a coarse representation of reality, which has many limitations and sources of uncertainty. Although the simulations correctly rank exposure, the quantitative agreement with experimental data is rather poor. The predicted ratio of exposure in the 90° to 180° position based on the tracer is 50 000; the corresponding value based on the aerosol trajectories is indeterminate; and the measured value is 26. The simulated value for the over-spray generation rate is nearly four times the measured value.

Implicit in the conduct of these simulations is that by matching the momentum–flux ratio of the experiment, one would obtain the same value of dimensionless concentration. Obviously such agreement was not observed. There are many possible explanations for the quantitative discrepancies noted above. However, the error in transfer efficiency is very important. Use of a 0.0254-m (1 in.) square orifice with a velocity of 35.56 m s^{-1} to simulate the actual impaction process leads to dramatic overestimation of the mass generation rate. Particles in the simulation do not have sufficient momentum to impact, and thus become available for exposure. This suggests that reducing the size of the orifice in the simulations, and increasing the air velocities (both jet and tunnel) to maintain the correct momentum flux ratio should produce better agreement with the experimental data. Research is currently underway to examine these refinements.

Comparability of the numerical predictions of aerosol concentration and size distribution with measured values is also problematic. Measured concentrations were gathered using open-face filters, while closed-face filters were used for the size distribution samples. These sampling methods will tend to underestimate the true aerosol concentration due to aspiration losses at the inlet, especially for larger particles. No attempt was made to account for these sampling losses in the numerical simulations. Using empirically derived equations for aspiration efficiency (Vincent, 1995) as a function of orientation, it is estimated that the true aerosol mass concentration ratio for the 90° to 180° case is at least twice the measured value of 26.

The superior agreement of the measured dimensionless concentration in the 90° case (0.14) with the simulation value using the tracer approach (0.2) versus the particle trajectory approach (1.08) may be related to this aspiration efficiency problem. If only smaller particles are sampled then their transport will be closer to the jet-air (tracer) than the larger particles. Calculating the dimensionless concentration for each size interval used in the simulation supports this hypothesis. These values increase in a nearly monotonic fashion from a value of 0.3 for a 2.5-μm particle to 1.9 for the 67.5-μm size.

The major computational limitation in this work relates to the enormous data files that must be generated to hold the particle trajectory data for subsequent processing. To calculate the converged

mean concentration using 2800 particles per size interval, over 60 gigabytes of data were processed in a very inefficient, time consuming manner. The fact that the source code is not available makes it impossible to include the post-processor as part of the FIDAP code. If this were possible, trajectory data would not need to be written to disk and post-processed, thus greatly improving the speed and capacity of this approach. At present we are investigating the creation of a more efficient post processor. This is critical since it appears that for lower concentrations more particles are needed to obtain convergent solutions. This has profound implications for the computational resources needed to obtain accurate concentrations in the range of interest for hygienists.

The use of computational fluid dynamics as a tool for occupational hygienists in exposure control is still in its infancy, but this work demonstrates a successful ranking of exposure using a relatively coarse level of simulation. The potential for CFD as a tool in the optimisation of control interventions is clear, and as computational resources improve more realistic simulations will be possible.

Acknowledgements—This work was supported by Grant Number R01/OH02858-06 from the U.S. National Institute of Occupational Safety and Health (NIOSH), and by the North Carolina Supercomputing Centre (NCSC). Its contents are solely the responsibility of the authors and do not necessarily represent the official views of NIOSH or NCSC. The authors would like to acknowledge the work of Mr Jordan L. Kovitz in assistance with the computer runs.

REFERENCES

Andersson, I.-M. and Alenius, S. (1997) Computational fluid dynamics as a design tool for contaminant control, (6-2). In *Ventilation '97 Global Developments in Industrial Ventilation*, Proceedings of the 5th International Symposium on Ventilation for Contaminant Control, eds H. Goodfellow and E. Tahti. CEIA ACIE, Ottawa, Canada.

Carlton, G. N. and Flynn, M. R. (1997a) A model to estimate worker exposure to spray paint mists. *Applied Occupational and Environmental Hygiene* **12**(5), 375–382.

Carlton, G. N. and Flynn, M. R. (1997b) Field evaluation of an empirical–conceptual exposure model. *Applied Occupational and Environmental Hygiene* **12**(8), 555–561.

FIDAP Manual (1995) Fluid Dynamics International, Evanston, IL.

Flynn, M. R., Gatano, B., McKernan, J. L., Dunn, K., Blazicko, B. A. and Carlton, G. N. (1999) Modeling breathing-zone concentrations of airborne contaminants generated during compressed air spray painting. *Annals of Occupational Hygiene* **43**(1), 67–76.

Heinonen, K., Kulmala, I. and Saamanen, A. (1996) Local ventilation for powder handling a combination of local supply and exhaust air. *American Industrial Hygiene Association Journal* **57**, 356–365.

Heinsohn, R. J. (1991) *Industrial Ventilation: Engineering Principles*. Wiley Interscience, New York.

Heinsohn, R. J., Johnson, D. and Davis, J. W. (1982) Grinding booth for large castings. *American Industrial Hygiene Association Journal* **43**(8), 587–595.

Heitbrink, W. A., Wallace, M. E., Bryant, C. J. and Ruch, W. E. (1995) Control of paint overspray in autobody repair shops. *American Industrial Hygiene Association Journal* **56**(10), 1023–1032.

Kim, K. Y. and Marshall, J. R. (1971) Drop-size distributions from pneumatic atomizers. *Association of Industrial and Chemical Engineers Journal* **17**(3), 575–584.

Kulmala, I., Saamanen, A. and Enbom, S. (1996) The effect of contaminant source location on worker exposure in the near-wake region. *Annals of Occupational Hygiene* **40**, 511–523.

Kwok, K.-C. (1991) A fundamental study of air spray painting. Ph.D. dissertation, University of Minnesota.

Nielsen, P. V., Restivo, A. and Whitelaw, J. H. (1978) The velocity characteristics of ventilated rooms. *Transactions of the American Society of Mechanical Engineers Journal of Fluids Engineering* **100**, 291–298.

Vincent, J. (1995) *Aerosol Science for Industrial Hygienists*. Pergamon Press, New York.